



The influence of catalyst acid strength on the methanol to hydrocarbons (MTH) reaction



Marius Westgård Erichsen, Stian Svelle, Unni Olsbye*

inGAP Centre of Research Based Innovation, Department of Chemistry, University of Oslo, N-0315 Oslo, Norway

ARTICLE INFO

Article history:

Received 16 November 2012

Received in revised form 5 March 2013

Accepted 14 March 2013

Available online 16 April 2013

Keywords:

Methanol conversion

MTH

H-SAPO-5

H-SSZ-24

Acid strength

Paring reaction

ABSTRACT

The methanol to hydrocarbons (MTH) reaction was studied over two isostructural zeotype catalysts of different acid strength, H-SAPO-5 and H-SSZ-24. Conversion of methanol alone was performed at 350–450 °C and WHSV = 0.31–2.48 h⁻¹. The product selectivities of the two catalysts were compared at similar conversion. The strongly acidic H-SSZ-24 was found to be more selective towards aromatic products and C₂–C₃ hydrocarbons as compared to the moderately acidic H-SAPO-5, which produced more non-aromatic C₄–C₈ hydrocarbons. Co-reactions of ¹³CH₃OH and benzene at 250–300 °C with low conversion of both reactants revealed that both catalysts produced ethene and propene from polymethylbenzenes via a paring mechanism. However, this reaction proceeded more readily in H-SSZ-24 than in H-SAPO-5. Furthermore, isobutene formation was found to be mainly associated with aromatic intermediates in H-SSZ-24, whereas isobutene produced over H-SAPO-5 was mainly formed via alkene intermediates. Overall, the results obtained in this study suggest that a lower acid strength promotes an alkene-mediated MTH reaction mechanism.

© 2013 Elsevier B.V. All rights reserved.

1. Introduction

Acid catalysis is important in many chemical reactions, not only in the petrochemical industry where acidic zeolite catalysts are used in major processes, such as in catalytic cracking [1]. Thus, the influence of acid strength on reaction mechanisms and rates is potentially an important topic. However, the term acidity in solids is somewhat ambiguous as both its definition and how to measure it has been a subject of debate [2]. In zeolites and related materials (zeotypes), the most important acid sites for catalysis are Brønsted type (proton donating). A calculated deprotonation energy for an isolated site is one measure of acid strength which has the advantage of being rigorously defined. Unfortunately, reliable deprotonation energies are not available for many zeotype catalysts. Another measure of acid strength is the interaction of the acidic OH group with basic probe molecules as monitored by e.g. vibrational spectroscopy [3] or NMR [2]. A recent study by Macht et al. [4] revealed that the activation barriers of both the dehydration of butanol and the isomerisation of hexane depended linearly on acid strength (quantified by deprotonation energy). However, the sensitivity to changing acid strength was different for the two reactions. This means that the selectivity of acid-catalysed

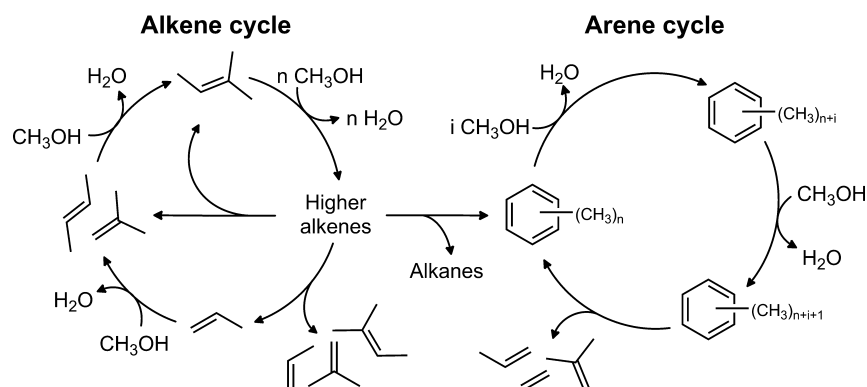
hydrocarbon reactions, where several classes of reactions compete, could be sensitive to a change in acid strength.

The conversion of methanol to hydrocarbons (MTH) over acidic zeotype catalysts is a flexible reaction route to produce light alkenes or gasoline from alternative hydrocarbon feedstocks such as natural gas, biomass or coal [5]. Several processes based on this reaction are being commercialised, such as the UOP/Hydro methanol to olefins (MTO) process, Lurgi's methanol to propene (MTP), Mobil's methanol to gasoline (MTG) process and the Topsøe TIGAS process [5]. Depending on catalyst used and conditions employed three main product groups, in addition to the simple dehydration of methanol to form dimethyl ether, can be obtained in these processes. These are: light alkenes such as ethene and propene; higher alkenes (C₄–C₈); and mixtures of aromatic and alkane products.

Direct reactions between methanol molecules are insignificant under steady-state MTH conditions [6,7]. Instead, product formation proceeds via a hydrocarbon pool mechanism [8–10]. The identity of the hydrocarbon pool has been studied intensively, and it has been found that both aromatics and alkenes are important hydrocarbon pool compounds [11–18]. The current mechanistic understanding of the MTH reaction is schematically illustrated in Scheme 1: Alkenes and aromatics are both methylated with methanol (or dimethyl ether) to form larger hydrocarbons and subsequently crack or dealkylate to form light alkenes and regenerate the starting compounds. This division between two classes of intermediates is often referred to as the dual-cycle concept. The two cycles are interrelated: Higher alkenes may undergo cyclisation

* Corresponding author. Tel.: +47 22855456.

E-mail address: unni.olsbye@kjemi.uio.no (U. Olsbye).



Scheme 1. General scheme of the dual-cycle mechanism. Both the relative propagation of each cycle and the exact structure of the intermediates depend on the catalyst employed and the reaction conditions. This in turn means that all products shown here are not necessarily observed in all systems.

and hydride transfer reactions leading to formation of aromatics and alkanes. Aromatics, on the other hand, contribute to formation of light alkenes that may subsequently take part in the alkene cycle. It has been found that the relative activity of the two classes of intermediates and their exact structure depends on the catalyst employed as well as the reaction conditions (see [5] and refs. therein): beta zeolite, with 12-ring zeolite channels, favour the heptamethylbenzenium cation as the aromatic reaction intermediate, leading preferably to formation of propene and isobutane [14,15,18–20]. MFI zeolites, with 3D 10-ring channels favour tri- and tetra-methylbenzene as aromatic intermediates, leading preferably to ethene and propene formation [16–19]. In each case, the alkene cycle contributes to product formation beside the arene cycle. TON, with 1D 10-ring channels of slightly smaller diameter than MFI, strongly favour the alkene cycle while the arene cycle is suppressed [21,22]. In addition to influencing which hydrocarbon pool species can be formed and converted, the available channel space inside the catalyst influences which products are able to diffuse out of the structure [23]. As such, the largest aromatic compound found in the product effluent of BEA is hexamethylbenzene, while in MFI it is 1,2,4,5-tetramethylbenzene. Aromatic compounds formed in TON are retained in the channels, and its effluent consists mainly of alkenes [5]. Evidence exists that a change in reaction conditions, or acid site densities, can change the relative propagation rates of the alkene and arene cycles [24,25]. However, the influence of acid strength on the MTH performance of the catalyst is not yet fully understood.

The effects of acid strength in MTH were first investigated by Yuen et al. [26], who compared aluminosilicate and silicoaluminophosphate versions of AFI (H-SAPO-5 versus H-SSZ-24) and CHA (H-SAPO-34 versus H-SSZ-13) structured catalysts. Their experiments were performed under similar conditions giving full conversion. They observed a more rapid breakthrough of methanol over the strongly acidic H-SSZ-13 than over the moderately acidic H-SAPO-34. Comparing the performance of the AFI and CHA topologies, they concluded that the pore-size was a more important factor than acid strength in this reaction. More recently, our group published a detailed comparison of H-SAPO-34 and H-SSZ-13 [27]. This study included a series of tests at less than full conversion at different temperatures, in addition to characterisation of the retained hydrocarbons after use. While it was found that H-SSZ-13 was more active and deactivated faster than the less acidic H-SAPO-34, the methanol conversion capacity (i.e. the cumulative methanol production before full deactivation) was surprisingly found to be higher in H-SSZ-13 at temperatures below 375 °C. Further mechanistic insights proved difficult due to the severe restrictions on diffusion in the CHA structure leading to a high degree of product shape selectivity [28].

In contrast to the CHA structure, where narrow pores restrict diffusion into and out of the large cavities, the AFI structure has one-dimensional tubular 12-ring channels that, while similar in diameter to the cavities of the CHA structure, are open all the way to the exterior. This allows bulky molecules to diffuse in and out of the structure, and provides an opportunity for monitoring and manipulating the hydrocarbon-pool by performing co-reaction experiments. Furthermore, the simple structure of the AFI framework makes it well-suited as a model system for the MTH reaction in general, as the absence of cavities and intersections facilitates estimation of the space available for reactions. In a recent study [29] we performed co-feeding and isotopic labelling experiments over the moderately acidic H-SAPO-5 catalyst (AFI structure, 12-ring pores) and found that this catalyst differed from large-pore zeolites studied previously. It was shown that aromatic polymethylbenzene (PolyMB) intermediates could produce ethene and propene under conditions where their concentration was high. However, we concluded that higher alkene intermediates were more important hydrocarbon pool species under normal MTH conditions. This conclusion contrasted previous findings over H-Beta, which has a similar pore size but is a stronger acid. In H-Beta, polyMBs were found to be the dominant intermediates [14,15,18,19] under similar conditions.

The present study is aimed to further elucidate the influence of acid strength of zeotype catalysts in the MTH reaction. For this purpose the zeolite analogue to H-SAPO-5, called H-SSZ-24, was synthesised and the performance of the two catalysts in MTH reaction was compared. Both product selectivities during methanol conversion and the reaction patterns of polyMBs in methanol/benzene co-reactions were investigated. Such a direct comparison between two isostructural catalysts of differing acid strength provides a unique opportunity to study the effect of acid strength alone.

2. Materials and methods

2.1. Catalyst synthesis and characterisation

H-SAPO-5 was synthesised hydrothermally from water, triethylamine (TEA) (Fluka, 99.5%), orthophosphoric acid (Merck, 85%), Cab-O-Sil M5 (Riedel-de Haen) and Catapal B (Vista). A mixture with the composition: $50\text{H}_2\text{O}:1\text{Al}_2\text{O}_3:1\text{P}_2\text{O}_5:0.1\text{SiO}_2:3.9\text{TEA}$ was prepared and crystallised for 4 h at 200 °C in a rotating Teflon lined steel autoclave. Removal of the structure directing agent (TEA) was performed by calcination in air at 600 °C for 2 h.

The synthesis of H-SSZ-24 was based on the work by Kubota et al. [30,31]. A sample of zeolite H-Beta was first synthesised according to [32] (without adding Ti) using water, tetraethylammonium

hydroxide (Aldrich, 40% in water), Cab-O-Sil M5 and aluminium nitrate ($\text{Al}(\text{NO}_3)_3 \cdot 9\text{H}_2\text{O}$, Fluka, 98%). This sample was then calcined at 550 °C (heating ramp ~50 °C/h) for 36 h and used as aluminium source in the synthesis of H-SSZ-24. The structure directing agent for H-SSZ-24 synthesis, N(16)-methylsparteinium hydroxide ($\text{MeSpa}^+\text{OH}^-$), was synthesised similarly to the procedure reported by Lobo et al. [33] and Kubota et al. [34]. Briefly, sparteine was extracted from (–)sparteine sulphate pentahydrate (ABCR) by stirring with 10% NaOH and extracting with CH_2Cl_2 . The solid (–)sparteine was then dissolved in acetone and methylated with methyl iodide (Sigma-Aldrich, 99%). The crude product was recrystallised from boiling 2-propanol and ion-exchanged to OH-form with Amberlite IRN 78 (Supelco) ion exchange resin.

The SSZ-24 sample was prepared by mixing 5.88 g of water, 2.27 g of a 0.66 mmol g⁻¹ solution of $\text{MeSpa}^+\text{OH}^-$ and 0.24 g of a 6.3 mmol g⁻¹ aqueous solution of NaOH. After stirring for 10 min, 0.18 g of the BEA precursor and 0.43 g Cab-O-Sil was added. This mixture was stirred for 4 h before being set to crystallise in a Teflon-lined steel autoclave at 170 °C for 25 h. The structure directing agent was removed by calcination at 550 °C (heating ramp ~50 °C/h) in a flow of 25% O₂ in N₂ for 10 h. The Na-SSZ-24 thus formed was ion-exchanged three times with an excess of 1 M NH₄NO₃ (30 g solution per gram catalyst) at 80 °C before calcining again at 550 °C in 25% O₂ in N₂ for 10 h again to make H-SSZ-24.

Both zeotype samples were characterised by powder XRD, SEM, N₂ adsorption, and FT-IR. For powder XRD measurements, a Bruker D8 Discover diffractometer with Bragg-Brentano geometry using Cu K α radiation ($\lambda = 1.5406 \text{ \AA}$) was employed. SEM was performed with a FEI Quanta 200 FEG-ESEM instrument. N₂ adsorption isotherms were measured at -196 °C, using a BELSORP-mini II instrument. Samples were outgassed in vacuum for 1 h at 80 °C and 3 h at 300 °C. Specific surface area was calculated using the BET equation based on p/p₀ data in the range 0.01–0.15. FT-IR measurements were performed in transmission mode on a Vertex 80 instrument with MCT detector. Before measurement the samples were pressed into a self-supporting wafer, and were pre-treated under vacuum by heating to 120 °C for 1 h, 300 °C for 1 h and 450 °C for 1 h.

2.2. Catalytic tests

All catalytic tests were performed in a fixed-bed glass reactor of 8 mm inner diameter. The catalyst powder was pressed and sieved to obtain particles between 0.25 and 0.42 mm. Prior to the introduction of reactants, for all experiments, the pressed and sieved catalyst was calcined in situ at 550 °C under a flow of oxygen for 1 h before cooling to reaction temperature. Reactants used were ¹²C methanol (VWR, 99.8%), ¹³C methanol (Cambridge Isotope Laboratories, 99%) and benzene (Riedel-de Haen, 99.5%). These reactants were fed over the catalyst by passing a stream of helium through a saturator at constant temperature.

Both catalysts were tested for the conversion of methanol at 350 °C and 450 °C. 100 mg of H-SAPO-5 and 25 mg of H-SSZ-24 was used. The methanol partial pressure in these experiments was 40 mbar (saturator temperature 0 °C) and the flow of helium was adjusted to obtain WHSV between 0.31 and 2.48 h⁻¹. Product selectivities in the effluent were compared for the two catalysts at similar conversion and temperature.

Co-reaction experiments of ¹²C benzene and ¹³C methanol were performed at feed partial pressures of 76 mbar and 25 mbar, respectively (saturator temperatures of 20 °C and 10 °C). 100 mg were used of both catalysts and WHSV was 1.0 and 0.8 h⁻¹ respectively over H-SAPO-5 and 8.0 and 6.4 h⁻¹ over H-SSZ-24. The effluents were analysed after 2 min on stream.

The reactor effluent was analysed quantitatively by online GC analysis (Agilent 7890 with flame ionisation detector) on a Restek

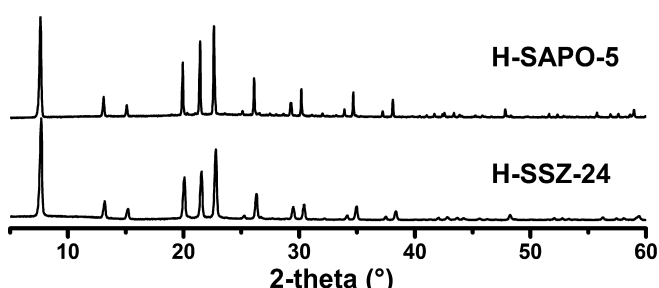


Fig. 1. Powder XRD patterns of the catalysts employed in this work.

Rtx®-DHA-150 column (150 m, 0.25 mm i.d., stationary phase thickness 1 μm). Hydrogen (purity 6.0) was used as carrier gas. For isotope analysis of effluent in the benzene/methanol co-feed experiments, the same GC and conditions were used, but the effluent was routed to an Agilent 5975C MS detector.

3. Results and discussion

3.1. Catalyst characterisation

Catalyst characterisation data are compiled in Table 1. X-ray diffraction patterns of H-SAPO-5 and H-SSZ-24 are shown in Fig. 1. Both diffractograms correspond to pure and highly crystalline AFI structures, only differing slightly in relative intensities and peak positions as expected due to the difference in composition. No crystalline impurities were detected. SEM analysis of the samples revealed the H-SAPO-5 samples to consist of hexagonal crystals roughly ~1 μm in diameter and 1–2 μm in length, while the H-SSZ-24 sample consisted of more irregular hexagonal rod-shaped crystals less than 1 μm long. The BET surface areas of the samples were determined to be 341 m²/g and 284 m²/g for H-SAPO-5 and H-SSZ-24 respectively.

EDS analysis of the two samples showed (Al+P)/Si = 80 for H-SAPO-5 and Si/Al = 35 in H-SSZ-24 (Table 1). These data suggest a higher density of acid sites in the zeolite sample. The consequences of this finding for the present study are discussed in Section 3.2 below.

FT-IR spectra of the H-SAPO-5 sample subjected to increasing amounts of CO at -196 °C are presented in Fig. 2. The activated sample (black line) shows three absorption bands in the O-H stretching region: at 3678, 3630 and at 3530 cm⁻¹. Similar bands in H-SAPO-5 have been described in numerous previous reports [35–38]. The band at 3678 cm⁻¹ is ascribed to P-OH groups at the external surface (or defect sites), while the two bands at 3630 and 3530 cm⁻¹

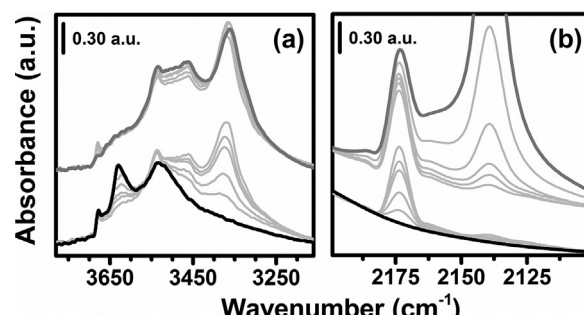


Fig. 2. FT-IR spectra of increasing dosages of CO on H-SAPO-5 at -196 °C. In (a) the OH stretching region is shown, while (b) shows the CO stretching region (background subtracted). The black bold curves correspond to the activated sample, while the grey bold curves correspond to the spectrum of highest CO loading.

Table 1

Summary of characterisation data for the two catalysts employed in this work. Acid site densities are the ratios of (Al+P)/Si (in H-SAPO-5) or Si/Al (in H-SSZ-24) as determined by EDS.

Sample	Structure	Crystal size (μm)	BET surface	Acid site density	$\nu(\text{OH})$ shift	$\nu(\text{CO})$ shift
H-SAPO-5	AFI	$1 \times 2 \mu\text{m}$	$340 \text{ m}^2/\text{g}$	80	-265 cm^{-1}	$+34 \text{ cm}^{-1}$
H-SSZ-24	AFI	$<1 \mu\text{m}$	$284 \text{ m}^2/\text{g}$	35	-317 cm^{-1}	$+38 \text{ cm}^{-1}$

are ascribed to bridging Si-OH-Al groups with protons located in the 12- and 6-rings of the AFI structure, respectively [36].

The grey lines in Fig. 2 are spectra of the catalyst samples exposed to CO. The O-H stretch region is shown in Fig. 2a. From Fig. 2a it can be seen that as CO is adsorbed on the sample, the Si-OH-Al band at 3630 cm^{-1} is eroded while two new bands grow at 3464 cm^{-1} and 3365 cm^{-1} . With a further increase in CO pressure, the P-OH band at 3678 cm^{-1} is also eroded. This change is accompanied by a decrease in intensity around 3500 cm^{-1} . It is uncertain whether these two events are related or not since several bands shift slightly as the CO loading increases. The appearance of two new bands when the Si-OH-Al band at 3630 cm^{-1} erodes is surprising since H-SAPO-5 is expected to contain only one type of strong acid site. This could mean either that two distinctly different acid sites are present in H-SAPO-5, or it could be due to a fermi-resonance effect similar to that proposed by Chakarova et al. [39] when they adsorbed CO on H-ZSM-5.

The corresponding spectra of the CO stretching region of the sample (Fig. 2b) mirror the observations above, as the CO stretching frequency is blue-shifted relative to free CO molecules when adsorbed on the acid sites of the materials. The frequency of CO adsorbed on the acidic Si-OH-Al groups are 2174 cm^{-1} , giving $\Delta\nu_{\text{CO}} = +34 \text{ cm}^{-1}$. The P-OH groups are, however, more difficult to observe in this region. The observation of only one band for CO adsorption at low coverage suggests that the observation of two bands in the OH region is spectral rather than representing two distinct sites.

IR spectra of H-SSZ-24 are presented in Fig. 3. The general spectroscopic features of H-SSZ-24 are very similar to those of H-SAPO-5: Three absorption bands are visible in the O-H stretching region of the activated H-SSZ-24 sample (black line), at 3747 , 3612 and 3488 cm^{-1} . These bands are ascribed to Si-OH groups and to Si-OH-Al groups located in 12- and 6-rings respectively. The band positions correspond well with those reported by Martinez-Triguero et al. [40] at room temperature, (in fact reproducing our measurements at room temperature gave complete overlap with their data). When the sample was cooled to -196°C , the values reported here were obtained. As CO is adsorbed (grey lines), the Si-OH-Al band at 3612 cm^{-1} is eroded and a new band grows at 3295 cm^{-1} . As more CO is adsorbed, the Si-OH band at 3747 cm^{-1} is also eroded, and a new band appears at 3650 cm^{-1} .

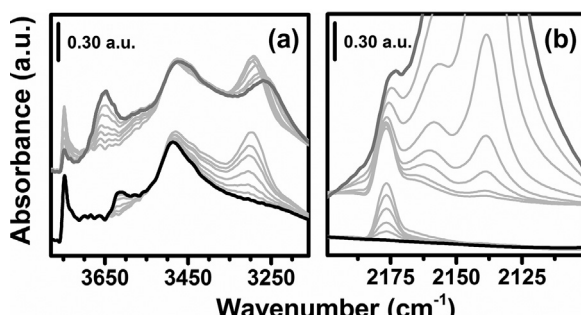


Fig. 3. FT-IR spectra of increasing dosages of CO on H-SSZ-24 at -196°C . In (a) the OH stretching region is shown, while (b) shows the CO stretching region (background subtracted). The black bold curves correspond to the activated sample, while the grey bold curves correspond to the spectrum of highest CO loading.

Again, the corresponding νCO region of the sample (Fig. 3b) mirrors the observations from the νOH region. The frequency of CO adsorbed on the acidic Si-OH-Al groups are 2177 cm^{-1} , giving $\Delta\nu_{\text{CO}} = +38 \text{ cm}^{-1}$. The interaction of the Si-OH groups in H-SSZ-24 with CO is also visible in the CO region, giving rise to a band at high CO coverage at around 2158 cm^{-1} .

Overall, the key difference between the H-SAPO-5 and H-SSZ-24 is the significant difference in magnitude of the shift in OH stretching frequency for the Si-OH-Al groups when they interact with CO. The largest shift observed in H-SAPO-5 is $\Delta\nu_{\text{OH}} = -265 \text{ cm}^{-1}$ while the shift in H-SSZ-24 is $\Delta\nu_{\text{OH}} = -317 \text{ cm}^{-1}$, meaning that the acid sites of H-SSZ-24 are significantly stronger than those of H-SAPO-5. Both this conclusion and the values of the shifts correspond fairly well with the differences found by Bordiga et al. [41] between the isostructural zeotypes H-SAPO-34 ($\Delta\nu_{\text{OH}} = -270 \text{ cm}^{-1}$) and H-SSZ-13 ($\Delta\nu_{\text{OH}} = -316 \text{ cm}^{-1}$), signifying that an acidity difference on this scale could be a general trend for high-silica zeolites and SAPO materials.

It is further interesting to note that in both samples the bridging Si-OH-Al groups present in the 6-rings of the AFI structure are not accessible to CO molecules at -196°C , as the bands at 3530 cm^{-1} in H-SAPO-5 and 3488 cm^{-1} in H-SSZ-24 do not disappear upon adsorption of CO. These sites have previously been shown to interact with stronger bases at higher temperatures [36,38], suggesting mobility of the protons involved. On the other hand, the Si-OH-Al groups in the 12-rings of the structure interact strongly with CO even at low coverage. The surface P-OH in H-SAPO-5 and Si-OH in H-SSZ-24 show a weak interaction with CO at high coverage only.

3.2. Methanol conversion over H-SSZ-24 and H-SAPO-5

The scope of this contribution was to elucidate the effects of a change in acid strength on the product selectivity and the favoured mechanism of the MTH reaction over wide pore zeotypes with AFI topology. Selectivity comparisons of the two catalysts at similar conversions (20 and 60%) at 350°C and 450°C are shown in Figs. 4 and 5, respectively. It should be noted that due to the activity differences between the two materials, the H-SSZ-24 sample was tested at four times higher weight hourly space velocity (WHSV) than the H-SAPO-5 sample in order to start at similar conversion. The employed WHSV for H-SSZ-24 and H-SAPO-5 was 2.48 h^{-1} and 0.62 h^{-1} respectively at 450°C , and 1.24 h^{-1} and 0.31 h^{-1} respectively at 350°C . For H-SAPO-5 at 350°C , data at low conversion was obtained in a separate experiment performed at WHSV 0.62 h^{-1} due to a very slow deactivation at WHSV 0.31 h^{-1} . Furthermore, the reported data are not initial conversions, but correspond to partly deactivated catalysts. Previous studies of H-SAPO-5 showed that deactivation had a negligible influence on the product selectivity versus methanol conversion correlations in the conversion ranges reported [29]. A similar conclusion has previously been reached for the title reaction both over H-ZSM-5 [42] and over several 1-dimensional 10-ring structures [43].

Distinct selectivity differences were observed between the two materials, exemplified in Figs. 4 and 5 at two conversion levels and two temperatures; i.e.; 20% and 60% conversion at 350°C and 450°C . A more detailed breakdown of the C_4 , C_5 and aromatics fractions from Figs. 4 and 5 is included as Supplementary material (section S1). Over H-SAPO-5, C_4 was the major product under all

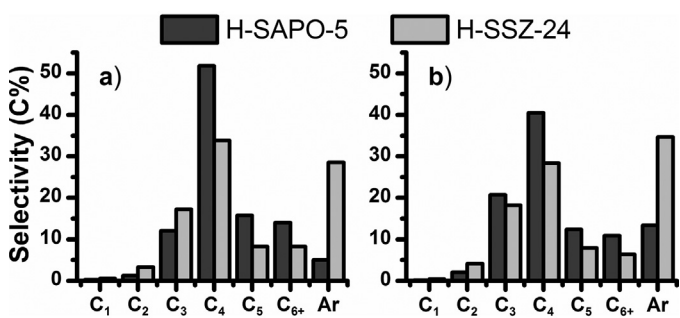


Fig. 4. Product selectivities for H-SAPO-5 (dark grey) and H-SSZ-24 (light grey) at 350 °C at 20% (a) and 60% (b) conversion. Data were obtained during deactivation of H-SSZ-24 at WHSV = 1.24 h⁻¹ and of H-SAPO-5 at WHSV = 0.62 h⁻¹ (a) and 0.31 (b).

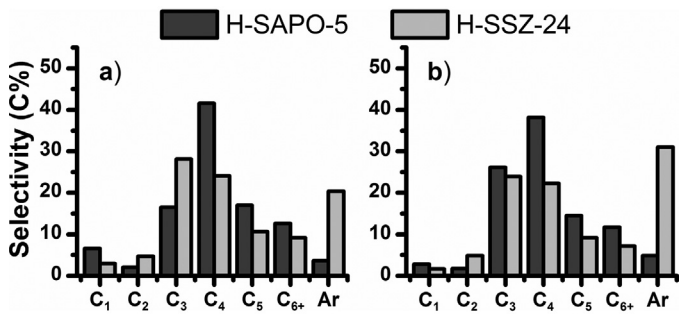


Fig. 5. Product selectivities for H-SAPO-5 (dark grey) and H-SSZ-24 (light grey) at 450 °C at 20% (a) and 60% (b) conversion. Data were obtained during deactivation of H-SSZ-24 at WHSV = 2.48 h⁻¹ and of H-SAPO-5 at WHSV = 0.62 h⁻¹.

conditions (~38–52% selectivity), with a volcano-like product distribution in the C₂–C₆₊ non-aromatic region. Isobutene represented >50% of the C₄ fraction under all reported conditions. Furthermore, H-SAPO-5 gave low selectivity to aromatic products; <14% at 350 °C and <5% at 450 °C, respectively, in the conversion range covered by the two figures. Turning to H-SSZ-24, its most distinct feature was a much higher selectivity to aromatic products than observed over H-SAPO-5. H-SSZ-24 gave >26% and >19% aromatics selectivity at 350 °C and 450 °C, respectively. Among the non-aromatic products, C₄ was the main fraction also over H-SSZ-24 at 350 °C, while C₃ was the main fraction at 450 °C. Isobutyl species dominated the C₄ fraction also over H-SSZ-24. In line with the higher selectivity towards aromatic products, a higher percentage of the non-aromatic products was paraffinic rather than olefinic over H-SSZ-24, compared to H-SAPO-5: At 350 °C, the C₄, C₅ and C₆₊ fractions of H-SSZ-24 were all composed of >60% isoalkanes, while the percentage of alkanes over H-SAPO-5 was 22% and 34%

in the C₄ and C₅ fractions, respectively, at the highest conversion (60%) and only around 10% at 20% conversion. At 450 °C, the amount of alkanes was even lower over H-SAPO-5 (<10%), while a significant alkane fraction was still found in the effluent of H-SSZ-24 (>40%).

Concerning the non-aromatic fraction, the relative percentages of the C₂–C₆ hydrocarbons were quite independent of conversion at each temperature over H-SSZ-24, but varied significantly with conversion over H-SAPO-5 (Figs. 4 and 5). The most striking example is the C₄:C₃ ratio, which changed from 4.3 at 20% conversion to 2.0 at 60% conversion over H-SAPO-5 at 350 °C, while it changed only from 2.0 to 1.6 over H-SSZ-24. At 450 °C, the corresponding numbers were: 2.5–1.5 for H-SAPO-5, and 0.9 at both conversions over H-SSZ-24.

Corresponding numbers for the C₃:C₂ ratio, was ~10 and 8–15 over H-SAPO-5 and 350 °C and 450 °C, respectively, and ~5 at 350 °C and 5–6 at 450 °C, over H-SSZ-24. The C₂ and C₃ fractions were under all conditions dominated by ethene and propene respectively. The C₄:C₂ ratio was significantly higher for H-SAPO-5 than for H-SSZ-24, being ≥20 over H-SAPO-5 and ≤10 over H-SSZ-24 under all reported conditions.

Overall, the data in Figs. 4 and 5 show that the selectivity to aromatic products is higher over H-SSZ-24 than over H-SAPO-5. The observed difference could be ascribed to the different acid strength of the two materials, but it could also be related to the higher density of acid sites in H-SSZ-24 compared to H-SAPO-5 (Table 1): a higher density of acid sites has previously been shown to favour sequential reactions when performing the MTH reaction over H-ZSM-5 for Si/Al ratios lower than 50 [42]. A similar influence of acid site density in propene oligomerisation over H-ZSM-5 has been reported for low Si/Al ratios, but Si/Al ratios of 40 and 140 gave very similar selectivity at a given conversion [44]. In order to elucidate the influence of acid site density on the selectivity pattern, a number of H-SAPO-5 batches with (Al+P)/Si ratios in the range 20–80 were tested and compared to H-SSZ-24. The test data are shown as Supplementary material, Figs. S1 and S2. Although individual selectivity differences were observed among the H-SAPO-5 batches, the selectivity towards aromatic products was distinctively higher over the H-SSZ-24 batch than over each of the H-SAPO-5 batches. The observed difference in selectivity towards aromatic products between H-SSZ-24 and H-SAPO-5 is therefore ascribed to the difference in acid strength between the two materials.

Yuen et al. have previously reported that H-SSZ-24 and H-SAPO-5 gave similar product selectivities in the MTH reaction, in apparent contradiction to our results. A possible reason for the difference is that their tests were performed at full conversion for all samples, allowing the products to undergo sequential reactions in the direction of thermodynamic equilibrium.

Table 2

Experimental details, conversion and product selectivities from co-reactions of ¹²C benzene and ¹³C methanol.

Temperature	250 °C		300 °C	
	H-SSZ-24	H-SAPO-5	H-SSZ-24	H-SAPO-5
WHSV benzene	6.4 h ⁻¹	0.8 h ⁻¹	6.4 h ⁻¹	0.8 h ⁻¹
WHSV methanol	8.0 h ⁻¹	1.0 h ⁻¹	8.0 h ⁻¹	1.0 h ⁻¹
Conversion (%)	7.5	1.8	21.0	16.1
Selectivity (%)				
Methane	0.4	0	0.2	0.1
C ₂	0.9	0.4	1.9	2.5
C ₃	1.9	1.2	4.2	6.7
C ₄	1.1	3.5	3.8	21.3
C ₅₊	5.0	1.7	3.6	17.7
Toluene	37.6	74.5	34.6	15.4
Other MBs	36.6	11.2	45.8	24.4
HexaMB	16.5	7.5	5.9	12.1

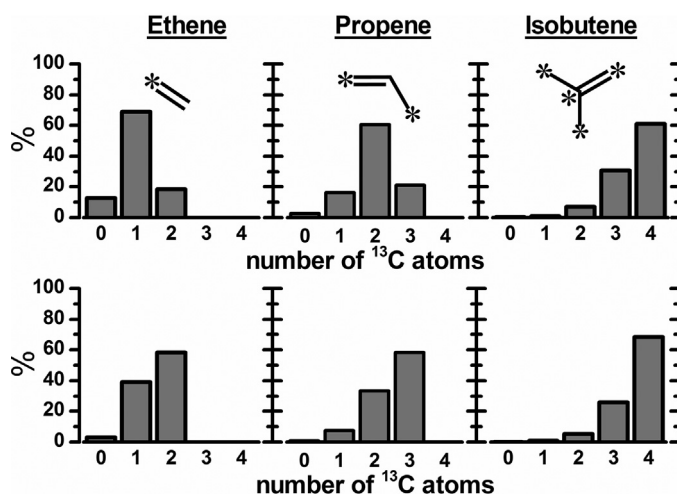


Fig. 6. Distribution of ¹³C atoms in ethene (left), propene (middle), isobutene (right) after 2 min of co-reacting methanol with benzene (molar ratio 3:1) at 250 °C (top) and 300 °C (bottom) over H-SAPO-5. At 250 °C, the total ¹³C content in ethene was 53% and 67% in propene, while it was 88% in i-butene. At 300 °C, the total ¹³C content was ~80% in ethene and propene and 91% in i-butene. The molecules above the graphs are drawn with stars signifying labelled carbon atoms representative of the most abundant isotopologues found at 250 °C.

3.3. Light alkene formation from aromatic intermediates

As presented in the Introduction, aromatic species represent both end products and hydrocarbon pool species in the MTH reaction. In order to investigate the reactivity of aromatic molecules in the two catalysts, co-feed experiments of ¹²C-benzene and ¹³C labelled methanol were performed at 250–300 °C. During these experiments the concentration of polymethylated benzene molecules (polyMBs) was greatly enhanced inside the catalysts compared to ordinary MTH experiments, thereby enabling an investigation of their reactivity. Again, a much higher WHSV of methanol and benzene combined was used over H-SSZ-24 than over H-SAPO-5. However, even with a factor 8 in contact time difference, significantly higher conversion was obtained over H-SSZ-24 (7.5%) compared to H-SAPO-5 (1.8%) after 2 min on stream at 250 °C (Table 2). At 300 °C the conversion after 2 min on stream was more similar over the two catalysts (21.0 vs. 16.1%), but relative polyMB yields differed significantly (Table 2). A short time on stream was necessary to obtain distinct isotopic labelling patterns in the products (Figs. 6 and 7). For this reason data collected after 2 min on stream are reported in spite of the conversion differences. It is apparent from Table 2 that, in line with the observations from conversion of methanol alone, H-SAPO-5 is much more selective towards isobutene/isobutane than H-SSZ-24. At 250 °C the ratios found between the yield of C₂, C₃ and C₄ hydrocarbons were 1:3:9 in H-SAPO-5, while they were 1:2:1 in H-SSZ-24. Upon increasing the temperature to 300 °C, these ratios did not change much, except for an increase in C₄ selectivity for H-SSZ-24, bringing the ratios to 1:2:2.

The isotopic distribution of the polyMBs produced by the co-reaction of ¹³C-methanol and ¹²C-benzene are shown as Supplementary material (Figs. S3–S6). The dominating isotopomer of all polyMBs contained the same number of ¹³C atoms as methyl groups. This is consistent with sequential methylations of benzene being the dominant pathway for formation of polyMBs under these conditions. However, it is worth noting that at 300 °C (Fig. S4), the ¹³C distribution in the polyMBs produced by H-SAPO-5 became bimodal. The surprisingly high abundance of highly ¹³C substituted isotopomers may suggest that formation of polyMBs from alkenes

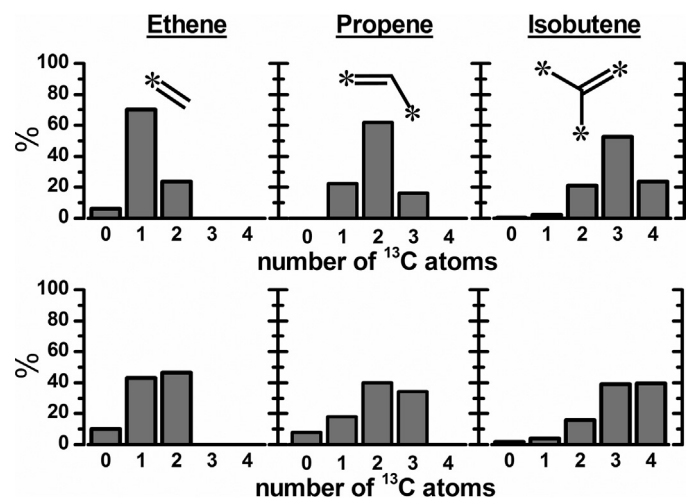


Fig. 7. Distribution of ¹³C atoms in ethene (left), propene (middle), isobutene (right) after 2 min of co-reacting methanol with benzene (molar ratio 3:1) at 250 °C (top) and 300 °C (bottom) over H-SSZ-24. At 250 °C, the total ¹³C content in ethene and propene was ~60%, while it was 75% in i-butene. At 300 °C total ¹³C contents was ~70% in ethene and propene and 78% in i-butene. The molecules above the graphs are drawn with stars signifying labelled carbon atoms representative of the most abundant isotopologues found at 250 °C.

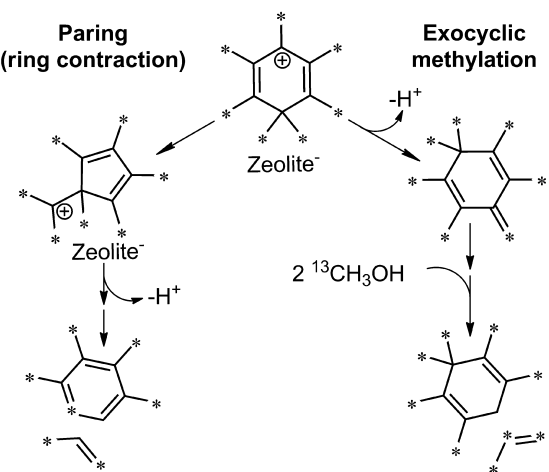
(originating mainly from methanol) is competitive with benzene methylation under these conditions.

The isotopic distribution in the light alkenes over H-SAPO-5 is shown in Fig. 6. It reveals that one ¹²C atom from benzene was incorporated into the ethene and propene produced over H-SAPO-5 at 250 °C. On the other hand the isobutene produced over this catalyst contained a significantly larger fraction of ¹³C atoms than the lighter compounds, and the all ¹³C isotopomer was dominant. At 300 °C, all alkenes contained more ¹³C and the all-¹³C isotopomer dominated in all three compounds. The systematic incorporation of ¹²C atoms originating from benzene in ethene and propene at 250 °C points to polyMBs as intermediates for the production of these alkenes. On the other hand, the lack of such a systematic pattern and the low incorporation of ¹²C in isobutene indicate that this alkene is formed by a mechanism different from the lighter alkenes in H-SAPO-5.

A plot of isotopic distribution in products formed over H-SSZ-24 is shown in Fig. 7. Similarly to what was found for H-SAPO-5 at 250 °C, the major isotopomers of ethene and propene contained one ¹²C atom. However, in contrast to H-SAPO-5, the dominating isobutene isotopomer also contained one ¹²C atom at this temperature. At 300 °C the alkenes contained a larger fraction of ¹³C atoms, and the isotopic distribution observed at 250 °C was less clear. However, a significant amount of alkenes containing one ¹²C atom was still observed. Overall, significantly more ¹²C was present in all three alkenes than what was found over H-SAPO-5 at both temperatures. These results suggest that C₂–C₄ alkene formation at 250 °C over H-SSZ-24 mainly proceeds through polyMB intermediates, and that this same mechanism contributes even at 300 °C.

3.4. On the mechanism of arene de-alkylation

The data reported in Figs. 6 and 7 further shed light on another mechanistic aspect of the MTH reaction: PolyMB de-alkylation. This topic has been debated for many years, and two main mechanistic proposals have been put forth: The paring reaction and the exocyclic methylation mechanism. A simplified scheme of these two reaction pathways is presented in Scheme 2. The latter mechanism was first proposed by Mole et al. [45,46] and later refined by Haw et al. [23] and involves deprotonation of HeptaMB⁺



Scheme 2. Expected labelling patterns when propene is split off from a selectively labelled heptaMB⁺ via paring or exocyclic mechanisms, respectively. Stars are used in order to keep track of the carbons originally present as methyl groups. The paring pathway involves systematic scrambling of these into the benzene ring, while the exocyclic methylation does not. Scheme from [29].

to form a neutral compound with an exocyclic double bond. This double bond can be methylated once or twice to form an ethyl or isopropyl side-chain, which is subsequently eliminated. On the other hand, the paring reaction, first proposed by Sullivan et al. [47] to account for the high yield of isobutene during hydrocracking of hexamethylbenzene, involves the rearrangement of HeptaMB⁺ to a five-membered ring with an alkyl substituent. This smaller ring can then either split off propene directly or reorganise further to eliminate isobutene before deprotonation and expansion back to a six-ring. Contrary to the exocyclic methylation mechanism, the paring reaction induces incorporation of ring carbons into the alkene product. In Scheme 2, the stars signify ¹³C-labelled carbon atoms, i.e. the carbons originally present as methyl groups. While Scheme 2 depicts HeptaMB⁺ as the main intermediate, similar mechanisms are assumed to exist for polymethylbenzenium cations with fewer methyl groups, and the labelling patterns are also expected to be similar if the elimination products are ethene or isobutene instead of propene (i.e. one unlabelled carbon should be observed in both alkenes if the paring mechanism dominates).

Looking back at Fig. 6, we observe that the labelling patterns of ethene and propene at 250 °C over H-SAPO-5 are consistent with a paring mechanism. In our recent study of this catalyst [29], we concluded from these data that these two alkenes could be formed by a paring-type mechanism, whereas isobutene was formed via an alkene methylation/cracking cycle even under co-feed conditions which strongly favour the propagation of the arene cycle. A cycle of successive alkene methylation and cracking reactions nicely explains the high abundance of ¹³C in isobutene, as the abundance of ¹³C would increase with each cycle if the starting molecule was e.g. ¹²C¹³C₂-propene. From Fig. 7, the labelling patterns of all three alkenes at 250 °C over H-SSZ-24 are seen to fit with a paring-type mechanism. It is noteworthy that this result is in full agreement with the propene and isobutane labelling patterns in similar experiments previously performed over H-Beta [15]. Since the labelling pattern of isobutene in H-SAPO-5 can be explained by the alkene cycle while all other alkenes display labelling patterns in accordance with the paring mechanism, a paring-type reaction involving systematic scrambling of ring-carbons appears responsible for all product formation in the arene cycle over these catalysts. While the de-alkylation mechanism does not necessarily proceed exactly as shown by the paring mechanism in Scheme 2, a

ring-contraction or -expansion step must be involved in the growth and elimination of alkyl side-chains.

3.5. Summary and mechanistic interpretations

The main findings of this study may be summarised as follows: In Section 3.2, it was found that the strongly acidic H-SSZ-24 is more selective towards ethene and aromatics than the moderately acidic H-SAPO-5 during methanol conversion. Furthermore, it was found that the relative distribution of C₂–C₄ alkenes was more sensitive to the conversion of methanol in H-SAPO-5 than in H-SSZ-24. This observation may suggest that C₂–C₄ alkenes are mainly formed from a common precursor in H-SSZ-24, but probably not in H-SAPO-5.

The co-feed experiments in Section 3.3 showed that H-SAPO-5 was significantly more selective towards isobutene than H-SSZ-24. Furthermore, as pointed out in Section 3.4, isobutene showed an isotopic labelling pattern consistent with an alkene cycle over H-SAPO-5, but with an arene cycle over H-SSZ-24 at 250 °C. C₂ and C₃ showed an isotopic labelling pattern consistent with formation from an arene cycle over both catalysts at 250 °C. These data match the selectivity patterns reported in Section 3.2 well, and point to the alkene cycle being a dominating source of product formation in H-SAPO-5, while the arene cycle dominates in H-SSZ-24.

If one further considers the data obtained at 300 °C, showing the transition from a clear labelling pattern at 250 °C to nearly complete scrambling for all alkenes in H-SAPO-5 (Fig. 6) at 300 °C, and compares it to the situation in H-SSZ-24, where the original pattern was still visible (Fig. 7) at the higher temperature, it strengthens the argument that polyMBs are less important hydrocarbon pool species in H-SAPO-5 than in H-SSZ-24. Finally, it should be noted that while these isotopic distributions were easily reproducible over a wide conversion range over H-SSZ-24 at 250 °C, obtaining paring-type labelling patterns in H-SAPO-5 required a very low conversion.

It has previously been suggested that the formation of the lightest alkenes, and especially ethene, is mainly associated with the arene cycle and polyMB intermediates [5]. In line with this suggestion, the observation of a higher C₃_a selectivity over the moderately acidic H-SAPO-5 than over the more strongly acidic H-SSZ-24 ties in nicely with the observed lower importance of polyMB intermediates during the co-feed experiments. As the two catalysts are very similar apart from their acid strength, it appears reasonable to conclude that a change in acid strength in turn leads to a shift in the relative abundance of the alkene or arene cycle, with a high acid strength favouring the latter cycle. It should be noted, however, that the co-feed experiments were conducted at a lower temperature than the methanol feed experiments, and that the relative abundance of the alkene versus the arene cycle in each material might be different at 350–450 °C than at 250–300 °C.

There are at least two possible explanations to the observed effect of acid strength in this work; i.e. the enhanced significance of the arene versus the alkene cycle to light alkene formation in H-SSZ-24 than in H-SAPO-5. Either, it could be an effect of the increased aromatics concentration, due to the higher selectivity towards aromatic products, in H-SSZ-24 (see Figs. 4 and 5). Computational studies suggest that cyclisation reactions are facile [48], meaning that hydride transfers are likely the rate-determining steps in the formation of aromatics. A link between acid strength and hydride transfers has been proposed previously [26,49], and could be at the core of the observed promotion of the arene cycle in H-SSZ-24. Another possibility is that the key reaction steps of the alkene and arene cycles display a different sensitivity to acid strength. Macht et al. [4] proposed that the main reason why n-hexane isomerisation is more sensitive to a change in acid strength than butanol dehydration is the more localised charge in the transition state

of the latter reaction compared to the former. It is plausible that the positive charges of transition states involving arenes are more diffuse than those involving alkenes, which could mean that the reactions of the arene cycle are more sensitive to acid strength than those of the alkene cycle.

From the data presented here it is not possible to conclude which, if either, of these two factors is most important, but the observation that it was difficult to propagate the arene cycle exclusively in H-SAPO-5 even during co-reactions of benzene and methanol (where the concentration of polyMBs is high) may suggest that the difference in the relative activity of the two classes of intermediates with acid strength are more important than the concentration of polyMBs.

4. Conclusions

Two isostructural zeolite catalysts with differing acid strength were tested in the MTH reaction, and it was found that the product mixtures formed were different in the two catalysts. In particular, the more strongly acidic H-SSZ-24 was more selective towards aromatics, ethene and propene than the moderately acidic H-SAPO-5. Co-feed experiments utilising ^{12}C benzene and ^{13}C methanol indicated differences in the preferred mechanism of alkene formation between the two catalysts. Together, these results led us to propose that the arene cycle is more important for product formation in the strongly acidic H-SSZ-24 than in the moderately acidic H-SAPO-5. Furthermore, the data imply that the acid strength may be used to tune the selectivity of zeotype catalysts towards aromatic and alkane versus alkene products.

Finally, the co-feed studies reported here strongly indicates that the main mechanistic pathway for alkene formation from polyMBs involves systematic scrambling of ring- and methyl-carbons. The best known mechanism of this type is the paring mechanism, but other ring-expansion or -contraction mechanisms are also feasible.

Acknowledgements

This publication is part of the inGAP Centre of Research-based Innovation, which receives financial support from the Norwegian Research Council under Contract No. 174893.

Appendix A. Supplementary data

Supplementary data associated with this article can be found, in the online version, at <http://dx.doi.org/10.1016/j.cattod.2013.03.017>.

References

- [1] T. Maesen, The Zeolite Scene, in: J. Čejka, H. van Bekkum, A. Corma, F. Schüth (Eds.), *Introduction to Zeolite Science and Practice*, Elsevier B.V., Amsterdam, 2007.
- [2] J.F. Haw, *Physical Chemistry Chemical Physics* 4 (2002) 5431–5441.
- [3] A. Zecchina, G. Spoto, S. Bordiga, *Physical Chemistry Chemical Physics* 7 (2005) 1627–1642.
- [4] J. Macht, R.T. Carr, E. Iglesia, *Journal of the American Chemical Society* 131 (2009) 6554–6565.
- [5] U. Olsbye, S. Svelle, M. Bjørgen, P. Beato, T.V.W. Janssens, F. Joensen, S. Bordiga, K.P. Lillerud, *Angewandte Chemie International Edition* 51 (2012) 5810–5831.
- [6] W.G. Song, D.M. Marcus, H. Fu, J.O. Ehrmann, J.F. Haw, *Journal of the American Chemical Society* 124 (2002) 3844–3845.
- [7] D. Lesthaeghe, V. Van Speybroeck, G.B. Marin, M. Waroquier, *Angewandte Chemie International Edition* 45 (2006) 1714–1719.
- [8] I.M. Dahl, S. Kolboe, *Catalysis Letters* 20 (1993) 329–336.
- [9] I.M. Dahl, S. Kolboe, *Journal of Catalysis* 149 (1994) 458–464.
- [10] I.M. Dahl, S. Kolboe, *Journal of Catalysis* 161 (1996) 304–309.
- [11] B. Arstad, S. Kolboe, *Journal of the American Chemical Society* 123 (2001) 8137–8138.
- [12] B. Arstad, S. Kolboe, *Catalysis Letters* 71 (2001) 209–212.
- [13] W.G. Song, J.F. Haw, J.B. Nicholas, C.S. Heneghan, *Journal of the American Chemical Society* 122 (2000) 10726–10727.
- [14] A. Sassi, M.A. Wildman, H.J. Ahn, P. Prasad, J.B. Nicholas, J.F. Haw, *Journal of Physical Chemistry B* 106 (2002) 2294–2303.
- [15] M. Bjørgen, U. Olsbye, D. Petersen, S. Kolboe, *Journal of Catalysis* 221 (2004) 1–10.
- [16] S. Svelle, F. Joensen, J. Nerlov, U. Olsbye, K.-P. Lillerud, S. Kolboe, M. Bjørgen, *Journal of the American Chemical Society* 128 (2006) 14770–14771.
- [17] M. Bjørgen, S. Svelle, F. Joensen, J. Nerlov, S. Kolboe, F. Bonino, L. Palumbo, S. Bordiga, U. Olsbye, *Journal of Catalysis* 249 (2007) 195–207.
- [18] S. Svelle, U. Olsbye, F. Joensen, M. Bjørgen, *Journal of Physical Chemistry C* 111 (2007) 17981–17984.
- [19] M. Bjørgen, F. Joensen, K.-P. Lillerud, U. Olsbye, S. Svelle, *Catalysis Today* 142 (2009) 90–97.
- [20] M. Bjørgen, S. Akyalcin, U. Olsbye, S. Benard, S. Kolboe, S. Svelle, *Journal of Catalysis* 275 (2010) 170–180.
- [21] S. Teketel, U. Olsbye, K.P. Lillerud, P. Beato, S. Svelle, *Microporous and Mesoporous Materials* 136 (2010) 33–41.
- [22] S. Teketel, S. Svelle, K.P. Lillerud, U. Olsbye, *ChemCatChem* 1 (2009) 78–81.
- [23] J.F. Haw, W.G. Song, D.M. Marcus, J.B. Nicholas, *Accounts of Chemical Research* 36 (2003) 317–326.
- [24] J.H. Ahn, B. Temel, E. Iglesia, *Angewandte Chemie International Edition* 48 (2009) 3814–3816.
- [25] D.A. Simonetti, J.H. Ahn, E. Iglesia, *Journal of Catalysis* 277 (2011) 173–195.
- [26] L-T. Yuen, S.I. Zones, T.V. Harris, E.J. Gallegos, A. Auoux, *Microporous Materials* 2 (1994) 105–117.
- [27] F. Bleken, M. Bjørgen, L. Palumbo, S. Bordiga, S. Svelle, K.P. Lillerud, U. Olsbye, *Topics in Catalysis* 52 (2009) 218–228.
- [28] B.P.C. Hereijgers, F. Bleken, M.H. Nilsen, S. Svelle, K.P. Lillerud, M. Bjørgen, B.M. Weckhuysen, U. Olsbye, *Journal of Catalysis* 264 (2009) 77–87.
- [29] M. Westgård Erichsen, S. Svelle, U. Olsbye, *Journal of Catalysis* 298 (2013) 94–101.
- [30] Y. Kubota, H. Maekawa, S. Miyata, T. Tatsumi, Y. Sugi, *Microporous and Mesoporous Materials* 101 (2007) 115–126.
- [31] H. Maekawa, Y. Kubota, Y. Sugi, *Chemistry Letters* 33 (2004) 1126–1127.
- [32] D. Cardoso, in: H. Robson (Ed.), *Verified Syntheses of Zeolitic Materials*, Elsevier, 2001, pp. 118–119.
- [33] R.F. Lobo, M.E. Davis, *Microporous Materials* 3 (1994) 61–69.
- [34] Y. Kubota, S. Tawada, K. Nakagawa, C. Naitoh, N. Sugimoto, Y. Fukushima, T. Hanaoka, Y. Imada, Y. Sugi, *Microporous and Mesoporous Materials* 37 (2000) 291–301.
- [35] J. Chen, P.A. Wright, S. Natarajan, J.M. Thomas, *Studies in Surface Science and Catalysis* 84 (1994) 1731–1738.
- [36] B. Zibrowius, E. Loffler, M. Hunger, *Zeolites* 12 (1992) 167–174.
- [37] S.G. Hedge, P. Ratnasamy, L.M. Kustov, V.B. Kazansky, *Zeolites* 8 (1988) 137–141.
- [38] F. Schuth, D. Demuth, B. Zibrowius, J. Kornatowski, G. Finger, *Journal of the American Chemical Society* 116 (1994) 1090–1095.
- [39] K. Chakarova, K. Hadjiivanov, *Journal of Physical Chemistry C* 115 (2011) 4806–4817.
- [40] J. Martínez-Triguero, M.J. Diaz-Cabafías, M.A. Camblor, V. Fornés, T.L.M. Maesen, A. Corma, *Journal of Catalysis* 182 (1999) 463–469.
- [41] S. Bordiga, L. Regli, D. Cocina, C. Lamberti, M. Bjørgen, K.P. Lillerud, *Journal of Physical Chemistry B* 109 (2005) 2779–2784.
- [42] F.L. Bleken, T.V.W. Janssens, S. Svelle, U. Olsbye, *Microporous and Mesoporous Materials* 164 (2012) 190–198.
- [43] S. Teketel, W. Skistad, S. Benard, U. Olsbye, K.P. Lillerud, P. Beato, S. Svelle, *ACS Catalysis* 2 (2012) 26–37.
- [44] A.N. Mlinar, P.M. Zimmerman, F.E. Celik, M. Head-Gordon, A.T. Bell, *Journal of Catalysis* 288 (2012) 65–73.
- [45] T. Mole, G. Bett, D. Seddon, *Journal of Catalysis* 84 (1983) 435–445.
- [46] T. Mole, J.A. Whiteside, D. Seddon, *Journal of Catalysis* 82 (1983) 261–266.
- [47] R.F. Sullivan, C.J. Egan, G.E. Langlois, R.P. Sieg, *Journal of the American Chemical Society* 83 (1961) 1156–1160.
- [48] M. Vandichel, D. Lesthaeghe, J. Van der Mynsbrugge, M. Waroquier, V. Van Speybroeck, *Journal of Catalysis* 271 (2010) 67–78.
- [49] N. Hazari, J.A. Labinger, V.J. Scott, *Journal of Catalysis* 263 (2009) 266–276.